文章编号: 1001-9014(2019)03-0269-07 DOI: 10.11972/j.issn.1001-9014.2019.03.002

A novel photodetector based on Graphene/InAs quantum dots /GaAs hetero-junction

HU Zhi-Ting[1,2], GAN Tao[3], DU Lei[1], ZHANG Jia-Zhen[1], XU Huang[1], HAN Sai-Lei[1,4], XU He-Liang[3], LIU Feng[2], CHEN Yong-Ping[3], CHEN Gang[1*]

(1. State Key Laboratory of Infrared Physics, Shanghai Institute of Technical Physics, Chinese Academy of Sciences, Shanghai 200083, China;
2. Shanghai Normal University, Shanghai 200234, China;
3. Key Laboratory of Infrared Imaging Materials and Detectors, Shanghai Institute of Technical Physics, Chinese Academy of Sciences, Shanghai 200083, China;
4. University of Shanghai for Science and Technology, School of Material Sciences, Shanghai 200093, China)

Abstract: Due to the ultra-high electron mobility, graphene has been proposed as a prospective candidate for the photodetection. Nevertheless the relatively low photo absorption limits its potential application. On the other hand, the semiconductor quantum dots has exhibited high quantum efficiency and strong optical absorption. A novel photodetector by the incorporation of graphene with InAs quantum dots on GaAs substrate has been proposed. The performance of the fabricated photodetector, such like photoresponse, dark current, and time response, have been extensively studied. The photodetector based on graphene/InAs QDs/GaAs hybrid hetero-junction demonstrated that for the visible range of 637 nm a responsivity of about 17.0 mA/W, and detectivity of 2.3×10^{10} cmHz$^{1/2}$ W^{-1}, with an on/off ratio of about 1×10^{3} could be achieved. For the near infrared range of 940 nm, an even higher responsivity of of 207 mA/W has been obtained. Moreover a stronger dependence of dark current, Schottky barrier height and ideality factor on temperature has also been observed.

Key words: Graphene, GaAs, quantum dots (QDs), heterostructure, Schottky junction
PACS: 78.67.Wj, 85.35.Be, 42.79.Pw, 85.30.Hi

基于石墨烯/铟砷量子点/砷化镓异质结新型光电探测器

胡之厅[1,2], 甘 桃[3], 杜 磊[1], 张家振[1], 徐 煌[1], 韩赛垒[1,4], 徐鹤靓[3], 刘 锋[2], 陈永平[3], 陈 刚[1*]

(1. 中国科学院上海技术物理研究所 红外物理国家重点实验室,上海 200083;
2. 上海师范大学,上海 200234;
3. 中国科学院上海技术物理研究所 红外成像材料和器件重点实验室,上海 200083;
4. 上海理工大学 材料科学与工程学院,上海 200093)

摘要: 研究了一种石墨烯/铟砷量子点/砷化镓界面形成的异质结探测器的暗电流特性以及光电响应性质. 虽然石墨烯具有很高的电子迁移率,但受限于较低的光子吸收率,使其在光电探测领域的应用受到了限制. 而半导体量子点具有量子效率高,光吸收能力强等独特优点. 于是利用石墨烯-砷化铟量子点-砷化镓异质结结构制备了一种新型光电探测器. 并对该探测器的响应率、*I-V* 特性曲线、暗电流特性、探测率、开关比等关键性能进行了研究. 其在637 nm入射光情况下的响应率、探测率以及开关比可分别达到为17.0 mA/W、2.3×10^{10} cmHz$^{1/2}$ W^{-1}和1×10^{3}. 而当入射光为近红外波段的940纳米时,响应率进一步增加到了207 mA/W. 同时,还证实了该器件的暗电流、肖特基势垒高度和理想因子对温度的都具有较高的依赖性都较强.

收稿日期: 2018-06-15, 修回日期: 2018-12-26 Received date: 2018-06-15, revised date: 2018-12-26
Foundation items: Supported by the National Natural Science Foundation of China (61474130, U1531109), the Natural Science Foundation of Shanghai (17142200100), and Chinese Academy of Sciences via Hundred Talents Program
作者简介(Biography): HU Zhi-Ting (1992-), male, born in Shangrao, Jiangxi Province, China. His research area involves semiconductor photodetectors. E-mail: huzhiting1227@sina.com
* 通讯作者(Corresponding author): E-mail: gchen@mail.sitp.ac.cn

(C)1994-2019 China Academic Journal Electronic Publishing House. All rights reserved. http://www.cnki.net

关 键 词:石墨烯;砷化镓;量子点;异质结构;肖特基结

中图分类号:TN29 文献标识码:A

Introduction

Graphene, an attractive two-dimensional material, has been intensively studied in applications of optoelectronics and photodetection[1-6]. However, due to the weaker optical absorption and the absence of a gain mechanism (the ability to generate multiple carriers from per incident photon), photodetectors with a desirable photoelectric performance depended on pure graphene cannot be achieved. On the other hand, photodetectors based on Schottky junctions can significantly enhance optical absorption and achieve a higher photoelectric response. Schottky junctions always form at the contact interface between metal or graphene and conventional semiconductor materials. So recently attention has been paid on Schottky junctions structure. In this structure, optical absorption occurs at the depletion layer of semiconductor materials. Due to the ultra-high charge mobility, graphene was always used as a conducting channel for the transport of charge carriers. Bartolomeo et al. have investigated graphene/semiconductor Schottky junctions and made an elaborative summary[7]. Tongay et al. systematically studied the characteristics of graphene/semiconductor Schottky junctions[8], and obtained a series of parameters for the graphene/semiconductor Schottky barrier heights. Furthermore, they predicted the Schottky junctions structure could be used for the underlying applications in photoelectric sensors. An et al. have discussed the mechanisms of the photodetectors based on graphene/Si Schottky junctions in a systematical way[9], which indicated a stronger dependence of spectral responsivity and photoresponsivity on Schottky junctions from experimental results. However, detectors based on Schottky junction are still limited by bulk semiconductor materials.

Gallium arsenide (GaAs) is a Ⅲ-Ⅴ semiconductor compound material, with a sphalerite structure similar to diamond and a direct band gap of 1.42 eV. The electron mobility in GaAs is quite high, which is six times more than that of silicon. And its electron saturated drift velocity is extremely high. There are lots of excellent photoelectric devices have been fabricated based on GaAs, such as photodiodes, sensors and photodetectors[10-17]. Taking graphene/GaAs Schottky junctions as an example, Babichev et al. have transferred CVD-grown graphene to the surface of GaAs substrate and studied the contact properties of graphene/GaAs Schottky junctions[18]. In the meantime, they discussed and analyzed the contacting properties between monolayer or multilayer graphene and different metals on GaAs substrate. Woszczyna *et al*. investigated the magnetic transport properties by transferring the exfoliated graphene onto GaAs substrate[19]. Luo et al. obtained a fast response and highly sensitive near-infrared photodetector through implementing a passivation treatment of the interface between graphene and GaAs[20]. Gamucci et al. found an abnormal Coulomb resistance in graphene/GaAs heterojunction at low temperature[21]. D. Tomer et al. studied the transport characteristics of carriers under a reverse bias in graphene/GaAs Schottky junction[22]. It indicated that Schottky barrier height significantly decreased with increasing reverse bias voltage. Moreover, they also discussed the inhomogeneity of Schottky barrier at the interface between graphene and GaAs, and further analyzed possible reasons for this phenomenon. Jie *et al*. even fabricated a solar cell based on graphene/GaAs Schottky junction, and the power conversion efficiency could reach 1.95 %[23].

On the other hand, quantum dots (QDs), due to the quantum confinement effect, have exhibited enormous potential for optoelectronic applications, such as solar cells, lasers and infrared photodetectors. In the graphene/QDs structures, optical absorption mainly occurs at the QDs layer. When light illuminates on this structure, it will produce multiple photo-generated carriers. Then the photo-generated carriers are transferred into graphene layer from the QDs layer. And the charge conservation in the graphene channel makes electron (hole) replenishment from source electrode as soon as an electron (hole) reaches drain electrode. Therefore, carriers could recirculate many times in the graphene channel, and ultimately produce photo-current. Moreover, it can achieve a tunable responsivity, response speed and spectral selectivity by adjusting sizes, shape and chemical composition of QDs. As a member of the most important semiconductors QDs, InAs/GaAs QDs have gained enormous attention recently. The photoluminescence (PL) spectrum and Raman spectrum of graphene/GeSi quantum dots[24] and graphene/InAs/GaAs quantum dots[25,26] hybrid heterostructures have been reported recently, respectively. These research indicated that the optical absorption and responsivity of these devices based on graphene/semiconductor Schottky junctions can be enhanced dramatically in the wavelength range of visible light and near infrared. Unfortunately, until now, photodetectors based on graphene/epitaxial quantum dots have rarely been reported.

In this work, we designed and fabricated a novel graphene/InAs QDs/GaAs photodetector, where the self-assembled quantum dots were grown by molecular beam epitaxy (MBE) method. Then the investigation focused on characteristics of dark current and photoelectric response of this detector was performed to explore its potential for optoelectronic applications. The main motivation is that when graphene sheets are transferred onto GaAs semiconductor substrate, it will cause a charge transfer between graphene and GaAs because of the difference of their Fermi levels. It ultimately leads to a built-in electric field formed at the interface between graphene and GaAs. So when the light illuminates on this structure, it will produce a much stronger optical absorption and photoelectric response.

(C)1994-2019 China Academic Journal Electronic Publishing House. All rights reserved. http://www.cnki.net

1 Experimental

Highly doped n-type GaAs, with doped concentration of 10^{18} cm^{-3}, was here used as the substrate. Procedures of the samples fabrication are elaborated by molecular beam epitaxy (MBE) method using RIBER32 MBE system. Here, it mainly includes three steps for fabricating substrate. Firstly, it involves the growth of GaAs buffer layer. GaAs buffer layer, with doped concentration of 10^{18} cm^{-3}, was roughly grown for 120 nm at the temperature of 600℃ after substrates were dealt with high temperature and deoxidation. Following next step is 15 periods growth of InAs quantum dots (QDs) layers and GaAs spacer layers. Meanwhile, each coverage of InAs QDs layers is 2.5 MLs (monolayers) and thickness of each GaAs spacer layer is 20 nm. Finally, it is the growth of 10 nm GaAs layer, which is used as a capping layer to prevent surface oxidation of QDs layer. Thus the prepared InAs QDs/GaAs sample was taken as the fundamental condition of graphene/InAs QDs/GaAs hybrid structure photodetector. After that the detector was fabricated based on the materials grown with MBE. The initial preparation process was the fabrication of ohmic contact. Here, we used the standard GaAs ohmic contact fabricated process. The expected patterns of metal electrodes (AuGe/Ni/Au 100/20/200 nm) were fabricated by UV photolithography, wet etching and electron beam evaporation. In this wet etching process, the standard GaAs etching solution (H_3PO_4: H_2O_2: H_2O = 40: 20: 400 ml) was used. In order to get a better ohmic contact, the metal electrodes go through the annealing treatment under high temperature. The annealed temperature and time are set at 380℃ and 30 s, respectively. After the completion of ohmic contact process, a 30 nm Al_2O_3 dielectric layer was deposited on this substrate by atomic layer deposition (ALD) method. We need to open a 40 × 40 μm^2 window, where graphene can contact with InAs QDs/GaAs. Through this window, it will form Schottky junction at the contact interface between graphene and InAs QDs/GaAs. This window is produced by etching Al_2O_3 dielectric layer through a buffered hydrofluoric acid (BHF). Then we transferred a monolayer graphene sheet onto this substrate, which initially was grown on copper foil. The specific transfer process of graphene is as follows: Firstly, a layer of PMMA was spin coated onto the graphene film. Then it was put into a solution of ferric chloride [$FeCl_3$] to etch the copper foil. After the copper foil is etched completely, it will be taken out and put into a dilute hydrochloric acid solution. The PMMA-covered graphene is subsequently fished out by GaAs substrate. Finally, it was put into acetone solution, isopropanol solution and deionized water to remove PMMA in sequence. The top metal electrodes (Cr/Au 5/70 nm) were fabricated by a standard UV photolithography and electron beam evaporation process.

2 Results and discussion

Figure 1a shows the schematic structure of the graphene/InAs QDs/GaAs hybrid hetero-junction photodetector. The active area (40 × 40 μm^2) of this device is defined with a window opened at the center of the Al_2O_3 dielectric layer. In Fig. 1b, a Raman spectroscopy of the monolayer graphene shows two strong peaks: 2D peak (2 680 cm^{-1}) and G peak (1 580 cm^{-1}), which indicates a high quality of the monolayer graphene since 2D/G intensity ratio is about 2.16. Scanning electron microscopy (SEM) diagram of InAs QDs/GaAs substrate is shown in Fig. 1(c). Moreover, the on-off ratio is determined to be ~ 1 × 10^3 from Figure 1(d).

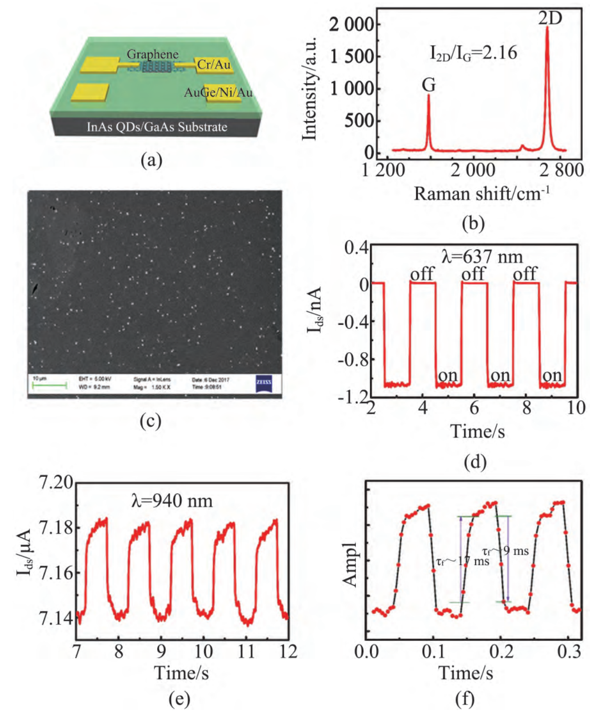

Fig. 1 (a) The 3D schematic for the fabricated device, (b) Raman spectrum of monolayer graphene, (c) Scanning electron microscopy (SEM) image of the as grown InAs QDs / GaAs substrate, (d) Time response of the device at zero bias (λ = 637 nm and P = 0.669 μW), (e) Time response of the device (λ = 940 nm), (f) Time response of the device (λ = 940 nm and f = 10 Hz)

图1 (a)该器件三维结构图,(b)单层石墨烯的拉曼光谱图,(c)InAs QDs /GaAs衬底的扫描电子显微镜图,(d)零偏压下探测器的时间相应(λ = 637 nm和P = 0.669 μW),(e)探测器的时间响应(λ = 940 nm),(f)探测器的时间响应(λ = 940 nm, f = 10 Hz)

Figure 2a shows the dark *I-V* characteristic curve over the temperature range of 80 ~ 200 K in the steps of 20 K, which presents a typical rectifying behavior. This is a consequence of the formation of Schottky junction at the interface between graphene and InAs QDs/GaAs substrate. As the graphene/InAs QDs/GaAs Schottky junction forms, electrons transfer into graphene from GaAs due to the Fermi energy difference. This causes electronic bands bending of GaAs, which lead to the formation of the built-in electric field at the graphene/GaAs interface. When the incident light illuminates on this structure, photogenerated carriers drift onsets driven by this electric field and produces photocurrent. Moreover, it is also observed that open circuit voltage increases with tempera-

(C)1994-2019 China Academic Journal Electronic Publishing House. All rights reserved. http://www.cnki.net

ture decreasing. This can be attributed to the reduction in thermal energy of electrons. Figure 2b shows the I-V characteristic curve under reverse bias at the temperature from 80 K to 200 K. The obvious rectification behavior implies that the classic thermionic emission theory can be used to describe the graphene/InAs QDs/GaAs heterostructure Schottky junction by the thermionic emission based diode equation:

$$I(T,V) = I_0(T)\left[\exp\left(\frac{eV}{nK_BT}\right) - 1\right] \quad , \quad (1)$$

where $I(T,V)$ is the current across the graphene/InAs QDs/GaAs interface, e is electron charge, K_B is the Boltzman constant, T is the absolute temperature, V is the applied voltage, n is the ideality factor, and I_0 is the reverse saturation current. Equation (1) also explains the increase in I with temperature increasing at a forward bias, while almost keeping a constant at a reverse bias. The reverse saturation current I_0 and ideality factor n can be obtained from the dark I-V characteristic curve at forward bias voltage from Figure 2a. By transforming Equation (1) into $\ln I = \ln I_0 + \frac{e}{nkT}V$ and fitting this curve under the forward bias, I_0 and n can be directly extracted from the y-intercept and the slope of the curve, respectively. According to the calculation results, n is about 6.50 at 80 K, and is 2.95 at 200 K. It is also clearly observed that n increases with temperature decreasing, as shown in Figure 2d. The ideality factor n greater than a normal value could be attributed to uneven surface. Due to the existence of InAs QDs layer, it cannot achieve an flat enough interface between graphene and InAs QDs/GaAs substrate. This could also lead to the inhomogeneity of Schottky barrier at the interface, which can also cause a non-uniformity distribution of the charge at the interface. Meanwhile, the transfering process of graphene may cause more additional defects, which may even deteriote the inhomogeneity of Schottky barrier height.

In principle, The Richardson constant A^* only depends on the material properties of semiconductor. In order to obtain the Schottky barrier height $\varnothing_B$, we used a typical Richardson plot of $\ln I_0/T^2$ vs $1\,000/T$ extracted from the reverse saturation current I_0, which can be expressed by $\ln(I_0T^2) = \ln(AA^*) - \frac{e\varnothing_B}{K_BT}$. According to the Richardson plot of $\ln(I_0T^2)$ vs $1000/T$, the Schottky barrier height $\varnothing_B$ can be obtained from the value of slope straightforwardly. As is shown in Figure 2c, the slope of the fitting curve gradually decreases with the temperature increasing. This means the Schottky barrier height decreases with temperature increasing. Here, this curve is fitted by a equation: $y = A_2 + \frac{(A_1 - A_2)}{1 + e^{\frac{(x-x_0)}{dx}}}$. According to the calculation results, Schottky barrier height $\varnothing_B$ is about 0.167 eV at 80 K, and is 0.385 eV at 200 K.

Afterwards we study the photoresponse of the graphene/InAs QDs/GaAs heterostructure photodetector. Here, the incident light is guided from a solid state laser to the four-probe device by using optical fiber, which has

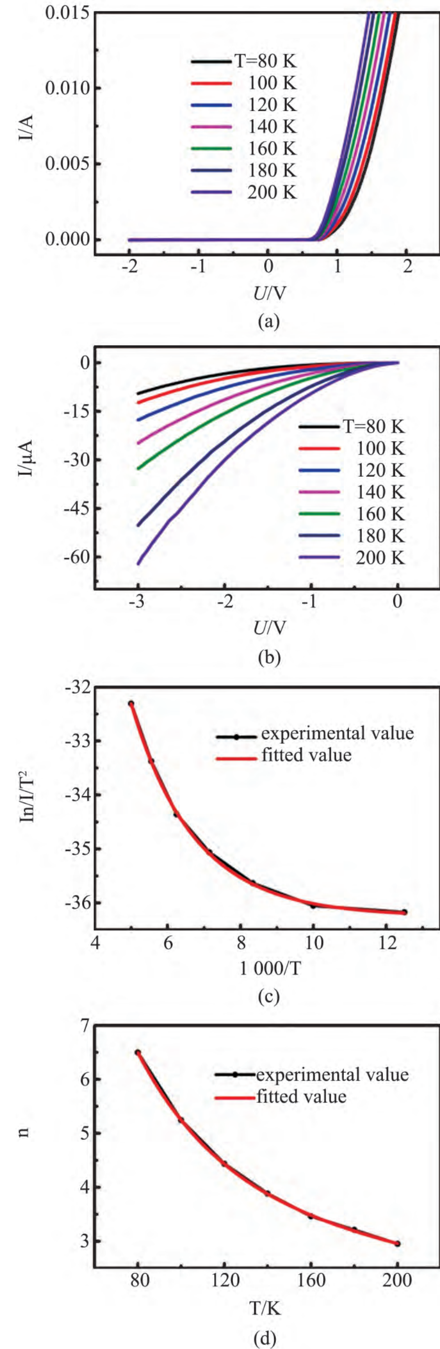

Fig. 2 Dark current characteristic curves of graphene/InAs QDs/GaAs heterostructure photodetector as a function of temperature (a) I-V characteristic curves measured with different temperature in the dark, (b) I-V cheracteristic curves at reverse bias voltage with different temperature, (c) Richardson plots of $\ln(I_0T^2)$ vs $(1\,000/T$, (d) Ideal factor n as a function of temperature

图2 石墨烯/铟砷量子点/砷化镓 异质结光电探测器与温度相关的暗电流特性曲线 (a) 无光照下,不同温度下的 I-V 特性曲线,(b) 反偏压下,不同温度下的 I-V 特性曲线,(c) 理查德森图 $\ln(I_0T^2)$ vs $(1000/T$,(d) 理想因子与温度的关系

an electron shield effect. Meanwhile, the incident wavelength $\lambda = 637$ nm and the optoelectronic properties of

(C)1994-2019 China Academic Journal Electronic Publishing House. All rights reserved. http://www.cnki.net

this device are characterized by Keithley 4200 electrical parameter analyzer. Figure 3a and 3b show the time response when the detector exposed to the light with different incident power and the *I-V* characteristic curve with/without light under the reverse bias, respectively. Photocurrent gradually increases with incident power increasing, which is caused by more incident photons with the higher incident power. More incident photons will produce more photo-generated carriers, which are contributed to a higher photocurrent. Figure 3(e) and Figure 3(f) show that the time response when the incident light wavelength $\lambda = 940$ nm. The rise time and fall time of this detetor are determined to be 17 ms and 9 ms, respectively, with the incident light frequence being set at 10 Hz, as is shown in Figure 3(f).

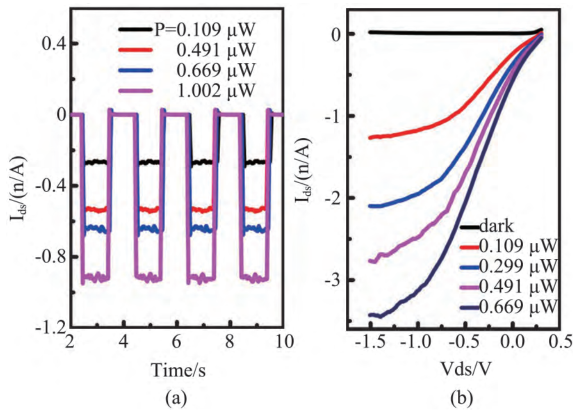

Fig. 3 (a) Time response of graphene/InAs QDs/GaAs heterostructure photodetector with different incident light power and drain-source voltage $V_{ds} = 0.1$ V, (b) *I-V* characteristic curve with/without light under the reverse bias

图 3 (a) 石墨烯/铟砷量子点/砷化镓异质结光电探测器在不同入射光功率下的时间响应,源漏电压 $V_{ds} = 0.1$ V, (b) 反偏压下,有/无光照的 *I-V* 特性曲线图

Responsivity and detectivity are the main performance parameters for a photodetector, which represent the ability for generating photocurrent per unit of the incident power and sensing weak signal, respectively. The two parameters can be described respectively as $R = \frac{I_{light} - I_{dark}}{P_{in}}$ and $D^* = \sqrt{\frac{A}{2eI_{dark}}}R$, where I_{light} is the current under illuminated, I_{dark} is the dark current, P_{in} the light incident power, A is the active area of this device ($40 \times 40\ \mu m^2$), and e is the electron charge, respectively. Based on Figure 1 d, R and D^* is estimated to be 4.6 mA/W and 2.29×10^{10} cm Hz$^{1/2}$ W^{-1} with the incident light of 637 nm at zero bias, respectively. Meanwhile, the time response of this device under different bias voltage is shown in Figure 4. One can see that photocurrent increases with the bias voltage increasing. And the responsivity of this device can reach about 17.0 mA/W at a reverse bias of −0.5 V with incident light $\lambda = 670$ nm. On the other hand, in figure 3e, when the detector exposed to the incident light with $\lambda = 940$ nm, it can produce a much stronger photocurrent. , the responsivity is determined to be 0.207 A/W, which can be attributed to the combined light absorption from both the graphene and the InAs QDs layer when the band gap of InAs QDs is about 870 nm.

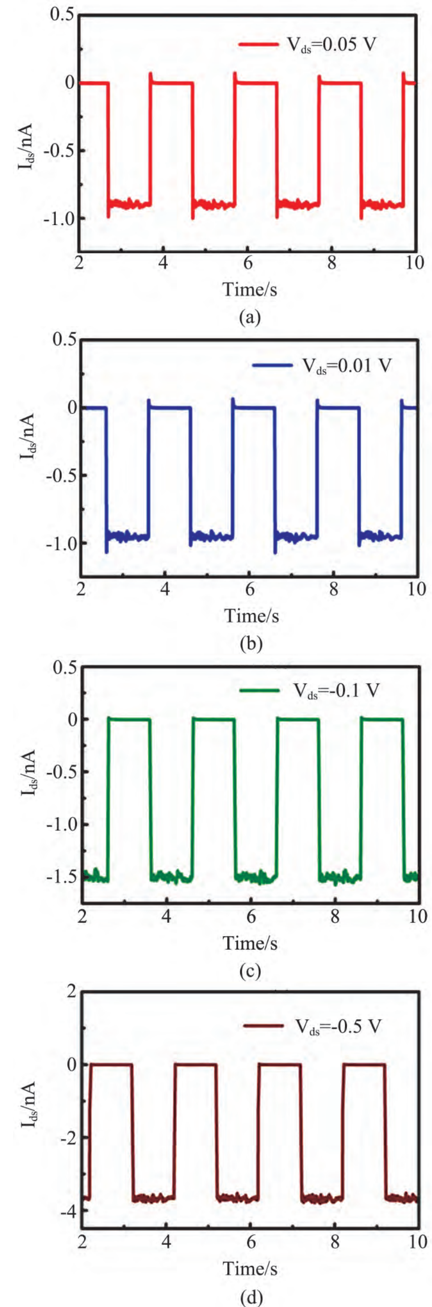

Fig. 4 Time respone of graphene/InAs QDs/GaAs heterostructure photodetector under different bias voltage (a) $V_{ds} = 0.05$ V, (b) $V_{ds} = 0.01$ V, (c) $V_{ds} = -0.1$ V, (d) $V_{ds} = -0.5$ V

图 4 石墨烯/铟砷量子点/砷化镓异质结光电探测器在不同偏压下的时间响应(a) $V_{ds} = 0.05$ V, (b) $V_{ds} = 0.01$ V, (c) $V_{ds} = -0.1$ V, (d) $V_{ds} = -0.5$ V

Unlike metal/semiconductor Schottky junctions, the work function of graphene is subjected to the effect of bias voltage because of the lower density of states. As is shown in Fig. 5a, the Fermi level of graphene and GaAs is described as $E_F(Gr)$ and $E_F(GaAs)$, respectively. Due to the Fermi level difference between graphene and GaAs, the system will reach an equilibrium state and the

(C)1994-2019 China Academic Journal Electronic Publishing House. All rights reserved. http://www.cnki.net

Fermi level of graphene and GaAs overlap at last without applied bias when the graphene sheet contacts with GaAs substrate. On the other hand, when forward or reverse bias are applied on graphene/GaAs Schottky junction structure, as shown in Fig. 5b and 5c, respectively, the Fermi level of graphene will shift down or up. Under forward bias, the graphene is positively charged and GaAs is negatively charged, which leads to a downward (upward) shift in Fermi level of graphene (GaAs). A downward shift of Fermi level of graphene can reduce the amount of photo-generated holes injected into graphene layer, which would further induce the decreasing of photocurrent. Vice verse, when a reverse bias is applied, a upward (downward) shift in Fermi level of graphene (GaAs) occurs. It would inject more photogenerated holes into the graphene from InAs QDs/GaAs layer, and hence, would greatly increase photocurrent. This may explain why the photocurrent can be lowered when applied a forward bias voltage, but elevated under a reverse bias for this device.

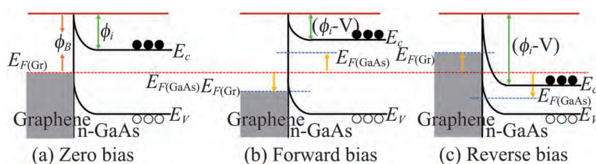

Fig. 5 Energy band diagrams of graphene/GaAs Schottky junction for (a) Zero bias, (b) Forward bias, (c) Reverse bias

图5 石墨烯/砷化镓肖特基结能带图(a)零偏压下,(b)正向偏压,(c)反向偏压

3 Conclusion

In summary, we fabricated a graphene/InAs QDs/GaAs photodetector, which exhibited significant rectifying characteristics and a stronger optical absorption. The photoresponse and dark *I-V* characteristic have been extensively studied under different condition. It has demonstrated that both of the Schottky barrier height and ideality factor have a stronger dependence on temperature The on-off ratio, photoresponsivity and detectivity of this detector can reach about 1×10^3, 4.6 mA/W and 2.29×10^{10} cmHz$^{1/2}$ W^{-1} at zero bias, respectively. Moreover, the responsity can be 17.0 mA/W when applied a reverse bias of −0.5 V. For the near infrared range of 940 nm, an higher responsivity of of 207 mA/W can be obtained. These results turn out that the inttroduction of the graphene/InAs QDs/GaAs heterostructure can form the Schottky junction structure at the interface between the graphene and the substrate, which can enhance the photo-absorption at both the visible and near infrared range, despite the uneven interface caused by the InAs QDs layer.

References

[1] Lewis G D A, ZHANG Yi, Schlenker C W, *et al*. Highly Flexible, and Transparent Graphene Films by Chemical Vapor Deposition for Organic Photovoltaics [J]. *ACS Nano*, 2010, **4**(5): 2865-2873.

[2] WANG Yu, XU Xiang-Fan, TONG Shi-Wun, *et al*. Interface Engineering of Layer-by-Layer Stacked Graphene Anodes for High-Performance Organic Solar Cells [J]. *Adv Mater*, 2011, **23**: 1514-1518.

[3] WU Xiao-Song, LI Xue-Bin, Sprinkle M, *et al*. De Heer. Epitaxial-Graphene/Graphene-Oxide Junction: An Essential Step towards Epitaxial Graphene Electronics [J]. *Physical Review Letters*, 2008, **101**: 026801.

[4] BAO Qiao-Liang, Loh K P. Graphene Photonics, Plasmonics, and broadband optoelectronic devices [J]. *ACS Nano*, 2012, **6**(5): 3677-3694.

[5] Bablich A, Kataria S, Lemme M. Graphene and Two-Dimensional Materials for Optoelectronic Applications [J]. *Electronics*, 2016, **5**(4): 13.

[6] Nguyen B H, Nguyen V H. Advances in graphene-based optoelectronics, plasmonics and photonics [J]. Advances in Natural Sciences: Nanoscience and Nanotechnology. 2016, 7(1): 013002.

[7] Bartolomeo A D. Graphene Schottky diodes: An experimental review of the rectifying graphene/semiconductor heterojunction [J]. *Physics Reports*, 2016, **606**: 1-58.

[8] Tongay S, Lemaitre M, Gila B, *et al*. Rectification at Graphene-Semiconductor Interfaces: Zero-Gap Semiconductor-Based Diodes [J]. *Physical Review X*, 2012, **2**: 011002.

[9] AN Xiao-Hong, LIU Fang-Ze, Yung J J, *et al*. Tunable Graphene? Silicon Heterojunctions for Ultrasensitive Photodetection [J]. *Nano Letter*, 2013, **13**: 909-916.

[10] WANG Hao. High gain single GaAs nanowire photodetector [J]. *Applied Physics Letters*, 2013, **103**: 093101.

[11] Cotal H, Fetzer C, Boisvert J, *et al*. III-V multijunction solar cells for concentrating photovoltaics [J]. *Energy Environ Sci.*, 2009, **2**(2): 174-192.

[12] Wasiak M, Walczak J, Motyka M, *et al*. Below-band-gap absorption in undoped GaAs at elevated temperatures [J]. *Optical Materials*, 2017, **64**: 137-141.

[13] Golovynskyi S, Seravalli L, Datsenko O, *et al*. Bipolar Effects in Photovoltage of Metamorphic InAs/InGaAs/GaAs Quantum Dot Heterostructures: Characterization and Design Solutions for Light-Sensitive Devices [J]. *Nanoscale Res Letter*, 2017, **12**(1): 559.

[14] CHEN Jun-Bao, XIA Wei, WANG Ming. Characteristic measurement for femtosecond laser pulses using a GaAs PIN photodiode as a two-photon photovoltaic receiver [J]. *Journal of Applied Physics*, 2017, **121**(22): 223103.

[15] Radziemska E. Thermal performance of Si and GaAs based solar cells and modules: a review [J]. *Progress in Energy and Combustion Science*, 2003, **29**(5): 407-424.

[16] Heshmat B, Pahlevaninezhad H, PANG Yuan-Jie, *et al*. Nanoplasmonic terahertz photoconductive switch on GaAs [J]. *Nano Letter*, 2012, **12**(12): 6255-6259.

[17] WANG Ai-Hua, SHI Yu-Lei, ZHOU Qing-Li, *et al*. Ultrafast terahertz emission properties in GaAs semiconductor [J]. *Proc. of SPIE*, 2015, **9625**: 962505.

[18] Babichev A V, Gasumyants V E, Egorov A Y, *et al*. Contact properties to CVD-graphene on GaAs substrates for optoelectronic applications [J]. *Nanotechnology*, 2014, **25**(33): 335707.

[19] Woszczyna M, Friedemann M, Pierz K, *et al*. Magneto-transport properties of exfoliated graphene on GaAs [J]. *Journal of Applied Physics*, 2011, **110**(4): 043712.

[20] LUO Lin-Bao, WANG Ming-Zheng, HU Han, *et al*. Near-Infrared Light Photovoltaic Detector Based on GaAs Nanocone Array/Monolayer Graphene Schottky Junction [J]. *Advanced Functional Materials*, 2014, **24**: 2794-2800.

[21] Gamucci A, Spirito D, Carrega M, *et al*. Anomalous low-temperature Coulomb drag in graphene-GaAs heterostructures [J]. *Nature Communication*, 2014, **5**: 5824.

[22] Tomer D, Raiput S, Hudy L J, *et al*. Carrier transport in reverse-biased graphene/semiconductor Schottky junctions [J]. *Applied Physics Letters*, 2015, **106**: 173510.

[23] JIE Wen-Jing, ZHENG Fen-Gang, HAO Jia-Hua. Graphene/gallium

(下转第289页)

(C)1994-2019 China Academic Journal Electronic Publishing House. All rights reserved. http://www.cnki.net

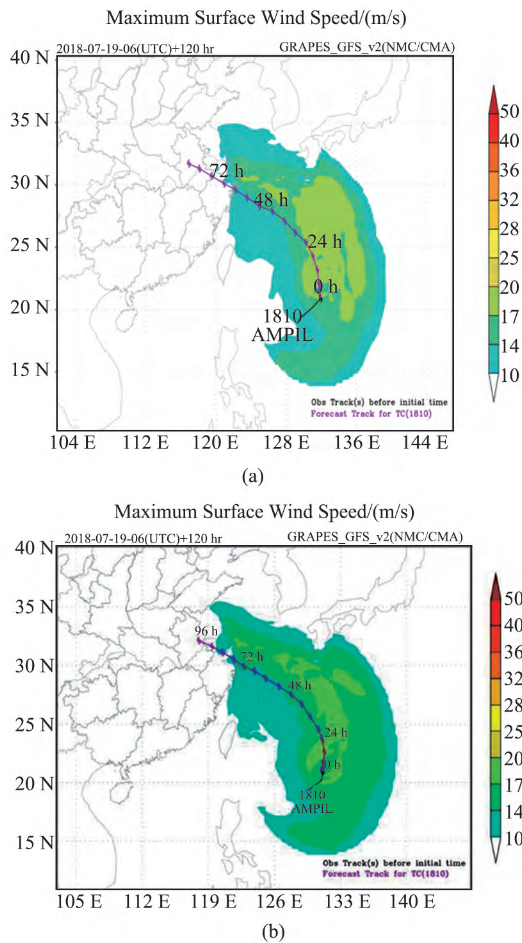

Fig. 6 forecast path of typhoon 'Ambi', (a) is a typhoon forecast path without assimilating GIIRS data, (b) is a typhoon forecast path with assimilating GIIRS data

图 6 台风"安比"的预报路径,(a) 未同化 GIIRS 资料预报路径,(b) 同化 GIIRS 资料预报路径

tion will directly serve short-term and imminent weather prediction enhance the timeliness of spectral detection and the ability of meteorological observation; broadening the detection spectrum, especially the long wave band (above 14 um), which will greatly enhance the ability of remote sensing information acquisition in China; by improving the spatial resolution and spectral resolution we can promote the ability of fine spectral resolution and meso-small scale meteorological observation.

4 Conclusion

It is the first time that the hyperspectral infrared atmospheric vertical sounder GIIRS is onboarded the FY-4 satellite. It can measure the atmospheric stratification information quantitatively and accurately on the vertical plane, which is equivalent to take a CT scan of the atmosphere. By detecting atmospheric temperature, humidity, atmospheric instability index etc, we can observe the occurrence of severe convective weather in advance[7].

For the first time in China, the real-time assimilation of the GIIRS data on FY-4A into the GRAPES Global Forecasting System has been realized, which has a significant impact on the current meteorological forecasting field, especially on the accuracy of typhoon intensity and track forecasts. The revolutionary progress of meteorological observation capacity will provide more significant meanings of early warning on disastrous weather and reducing the economic losses.

References

[1] WANG Zhan-Hu. Study on Optical System of Space-borne Interferometric Vertical Atmosphere Sounder [D]. Shanghai Institute of Technical Physics(**王战虎,星载干涉式大气垂直探测仪光学系统研究. 上海技术物理研究**), 2010.

[2] HUA Jian-Wen, MAO Jian-Hua. "No. 4 Feng Yun" Meteorological Satellite Atmospheric Vertical Sounder [J]. *Science*(**华建文, 毛建华. "风云四号"气象卫星大气垂直探测仪. 科学**), 2018, **70**(1): 24-29.

[3] LI De-Ren. Discussion on "Internet plus" space-based information service [J]. *Journal of remote sensing* (**李德仁. 论"互联网 + "天基信息服务. 遥感学报**), 2016, **20**(5): 708-715.

[4] SONG Jin-Yuan, Simulation study of retrieving clear sky atmospheric profiles using AIRS data [D]. Nanjing university of information science and technology (**宋金暖,AIRS 资料反演晴空大气廓线方法的模拟研究. 南京信息工程大学**), 2007.

[5] DAI Zuo-Xiao. Spatial Fourier spectrometer [D]. Shanghai Institute of Technical Physics(**代作晓,空间傅立叶分光探测仪. 海技术物理研究所**), 2004.

[6] FY-4 new data improve "Ambi" path forecast (**风云四号全新资料改进"安比"路径预报** [N/OL]. China Meteorological Administration (**中国气象局**). [2018-07-23]. http://www.cma.gov.cn/2011xwzx/2011xqxxw/2011xqxyw/201807/t20180723_474381.html.

[7] ZHOU Ai-Ming. Experimental study on retrieving atmospheric temperature and humidity profiles based on FY-4 hyperspectral infrared simulation data [D]. Nanjing university of information science and technology (**周爱明. 基于风云四号高光谱红外模拟资料反演大气温湿廓线试验研究. 南京信息工程大学**), 2017.

(上接第 274 页)

arsenide-based Schottky junction solar cells [J]. *Applied Physics Letters*, 2013, **103**: 233111.

[24] CHEN Yu-Lu, WU Qiong, MA Ying-Jie, *et al*. Plasmon-gating photoluminescence in graphene/GeSi quantum dots hybrid structures [J]. *Scientific Reports*, 2015, **5**: 17688.

[25] Ajlani H, Oueslati M, Cavanna A, *et al*. Graphene-capped InAs/GaAs quantum dots [J]. *Journal of Vacuum Science & Technology B*, 2013, **31**: 020602.

[26] Bkakri R, Kusmartseva O E, Kusmartsev F V, *et al*. Charge transfer properties in P3HT: graphene capped InAs/GaAs QDs hybrid heterostructure for photovoltaic application [J]. *Synthetic Metals*, 2015, **203**: 74-81.

(C)1994-2019 China Academic Journal Electronic Publishing House. All rights reserved. http://www.cnki.net